

# Superconductivity in type II layered Weyl semi-metals

B. Rosenstein<sup>1</sup> and B. Ya. Shapiro<sup>2</sup>

<sup>1</sup>*Department of Electrophysics, National Yang Ming Chiao Tung University, Hsinchu, Taiwan, R.O.C.*

<sup>2</sup>*Department of Physics, Institute of Superconductivity, Bar-Ilan University, 52900 Ramat-Gan, Israel.*

Novel "quasi two dimensional" typically layered (semi) metals offer a unique opportunity to control the density and even the topology of the electronic matter. In intercalated  $MoTe_2$  type II Weyl semi - metal the tilt of the dispersion relation cones is so large that topologically of the Fermi surface is distinct from a more conventional type I. Superconductivity observed recently in this compound [Zhang et al, 2D Materials **9**, 045027 (2022)] demonstrated two puzzling phenomena: the gate voltage has no impact on critical temperature,  $T_c$ , in wide range of density, while it is very sensitive to the inter - layer distance. The phonon theory of pairing in a layered Weyl material including the effects of Coulomb repulsion is constructed and explains the above two features in  $MoTe_2$ . The first feature turns out to be a general one for any type II topological material, while the second reflects properties of the intercalated materials affecting the Coulomb screening.

## INTRODUCTION.

The 3D and 2D topological quantum materials, such as topological insulators and Weyl semi - metals (WSM), attracted much interests due to their rich physics and promising prospects for application in electronic and spinotronic devices. The band structure in the so called type I WSM like graphene[1], is characterized by appearance linear dispersion relation (cones around several Dirac points) due to the band inversion. This is qualitatively distinct from conventional metals, semi - metals or semiconductors, in which bands are typically parabolic. In type-II WSM [2], the cones have such a strong tilt,  $\kappa$ , so that they exhibit a nearly flat band and the Fermi surface "encircles" the Brillouin zone, Fig.1b, Fig.1c. It is topologically distinct from conventional "pockets", see Fig.1a. This in turn leads to exotic electronic properties different from both the those in both the conventional and in the type I WSM. Examples include the collapse of the Landau level spectrum in magnetoresistance [3], and novel quantum oscillations [4].

The type II topology of the Fermi surface was achieved in particular in transition metal dichalcogenides [5]. Very recently  $MoTe_2$  layers intercalated by ionic liquid cations were studied[6]. The tilt value was estimated to as high as  $\kappa = 1.3$  that places it firmly within the type II WSM class. The measurements included the Hall effect and the resistivity at low temperatures demonstrating appearance of superconductivity. They discovered two intriguing facts that are currently under discussion. First changing the gate voltage (chemical potential) surprisingly has no impact on critical temperature,  $T_c$ , in wide range of density of the electron gas. Second  $T_c$  turned out to be very sensitive to the inter - layer distance  $d$ : it increases from 10.5Å to 11.7Å, while the critical temperature jumps from 4.2K to 7K. In the present paper we propose a theoretical explanation of these observations based on appropriate generalization of the conventional superconductivity theory applied to these materials.

Although early on unconventional mechanisms of superconductivity in WSM have been considered, accumulated experimental evidence points towards the conventional phonon mediated one [7–9]. In the previous paper[11] and a related work[10] a continuum theory of conventional superconductivity in WSM was developed. Magnetic response in the superconducting state was calculated[10][12]. The model was too "mesoscopic" to describe the type II phase since the *global* topology of the Brillouin zone was beyond the scope of the continuum approach. Therefore we go beyond the continuum model in the present paper by modeling a type II layered WSM using a tight binding approach. The in-plane electron liquid model is similar to that of graphene oxide[13] and other 2D WSM. It possesses a chiral symmetry between two Bravais sublattices for all values of the tilt parameter  $\kappa$ , but lacks hexagonal symmetry. The second necessary additional feature is inclusion of Coulomb repulsion.

It turns out that the screened Coulomb repulsion significantly opposes the phonon mediated pairing. Consequently a detailed RPA theory of screening in a layered material[14] is applied. We calculate the superconducting critical temperature taking into consideration the modification of the Coulomb interaction due to the dielectric constant of intercalator material and the inter-layered spacing  $d$ . The Gorkov equations for the two sublattices system are solved without resorting to the mesoscopic approach. Moreover since screening of Coulomb repulsion plays a much more profound role in quasi 2D materials the pseudo-potential simplification developed by McMillan[15] is not valid.

Rest of the paper is organized as follows. In Section II the microscopic model of the layered WSM is described. The RPA calculation of both the intra- and inter - layer screening is presented. In Section III the Gorkov equations for the optical phonon mediated intra- layer pairing for a multiband system including the Coulomb repulsion is derived and solved numerically. In Section IV the phonon theory of pairing including the Coulomb repulsion for a layered material is applied to recent extensive experiments on  $MoTe_2$ . The effect of intercalation and density on superconductivity is studied. This explains the both remarkable features of  $T_c$  observed[6] in  $MoTe_2$ . The last Section contains conclusions and discussion.

## A "GENERIC" LATTICE MODEL OF LAYERED WEYL SEMI-METALS

### Intra- layer hopping

A great variety of tight binding models were used to describe Weyl (Dirac) semimetals in 2D. Historically the first was graphene (type I,  $\kappa = 0$ ), in which electrons hop between the neighboring sites of the honeycomb lattice. We restrict the discussion to systems with the minimal two cones of opposite chirality and negligible spin orbit coupling. The two Dirac cones appear in graphene at  $K$  and  $K'$  crystallographic points in BZ. Upon modification (more complicated molecules like graphene oxide, stress, intercalation) the hexagonal symmetry is lost, however a discrete chiral symmetry between two sublattices, denoted by  $I = A, B$ , ensures the WSM. The tilted type I and even type II (for which typically  $\kappa > 1$ ) crystals can be described by the same Hamiltonian with the tilt term added. This

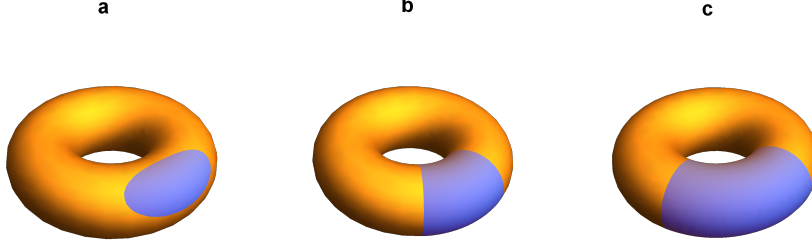


FIG. 1. Two distinct topologies of the Fermi surface in 2D. Topology of the 2D Brillouin zone is that of the surface of 3D toroid. On the left the “conventional” type I pocket is shown. In the center and on the right the type II topology is shown schematically. The filled states are in blue and envelop the torus. Despite the large difference in density of the two the Fermi surface properties like density of states are the same.

2D model is extended to a layered system with inter - layer distance  $d$ . Physically the 2D WSM layers are separated by a dielectric material with inter - layer hopping neglected, so that they are coupled electromagnetically only[14].

The lateral atomic coordinates are still considered on the honeycomb lattice are  $\mathbf{r}_n = n_1 \mathbf{a}_1 + n_2 \mathbf{a}_2$ , where lattice vectors are:

$$\mathbf{a}_1 = \frac{a}{2} (1, \sqrt{3}); \quad \mathbf{a}_2 = \frac{a}{2} (1, -\sqrt{3}), \quad (1)$$

despite the fact that hopping energies are different for jumps between nearest neighbors. Each site has three neighbors separated by  $\delta_1 = \frac{1}{3}(\mathbf{a}_1 - \mathbf{a}_2)$ ,  $\delta_2 = -\frac{1}{3}(2\mathbf{a}_1 + \mathbf{a}_2)$  and  $\delta_3 = \frac{1}{3}(\mathbf{a}_1 + 2\mathbf{a}_2)$ , in different directions. The length of the lattice vectors  $a$  will be taken as the length unit and we set  $\hbar = 1$ . The hopping Hamiltonian including the tilt term is[13, 16]:

$$K = \frac{\sqrt{3}}{4} \sum_{\mathbf{n}l} \left\{ \gamma \left( \psi_{\mathbf{n}l}^{sA\dagger} \psi_{\mathbf{r}_n + \delta_1, l}^{sB} + \psi_{\mathbf{n}l}^{sA\dagger} \psi_{\mathbf{r}_n + \delta_2, l}^{sB} + t \psi_{\mathbf{n}l}^{sA\dagger} \psi_{\mathbf{r}_n + \delta_3, l}^{sB} \right) + \text{h.c.} - \kappa \psi_{\mathbf{n}l}^{sI\dagger} \psi_{\mathbf{r}_n + \mathbf{a}_1, l}^{sI} - \mu n_{\mathbf{n}, l} \right\}. \quad (2)$$

Here an integer  $l$  labels the layers. Operator  $\psi_{\mathbf{n}l}^{sA\dagger}$  is the creation operators with spin  $s = \uparrow, \downarrow$ , while the density operator is defined as  $n_{\mathbf{n}l} = \psi_{\mathbf{n}l}^{sI\dagger} \psi_{\mathbf{n}l}^{sI}$ . The chemical potential is  $\mu$ , while  $\gamma$  is the hopping energy for two neighbors at  $\delta_1, \delta_2$ . Since the system does not possess hexagonal symmetry (only the chiral one), the third jump has the different hopping[13]  $t\gamma$ . Dimensionless parameter  $\kappa$  determines the tilt of the Dirac cones along the  $\mathbf{a}_1$  direction[16]. In the 2D Fourier space,  $\psi_{\mathbf{n}l}^{sA} = N_s^{-2} \sum_{\mathbf{k}} \psi_{\mathbf{k}l}^{sA} e^{-i\mathbf{k} \cdot \mathbf{r}_n}$ , one obtains for Hamiltonian (for finite discrete reciprocal lattice

$N_s \times N_s$ ):

$$K = N_s^{-2} \sum_{\mathbf{k}l} \psi_{\mathbf{k}l}^{s\dagger} M_{\mathbf{k}} \psi_{\mathbf{k}l}^s. \quad (3)$$

Here  $\mathbf{k} = \frac{k_1}{N_s} \mathbf{b}_1 + \frac{k_2}{N_s} \mathbf{b}_2$  (reciprocal lattice vectors are given in Appendix A) and matrix  $M_{\mathbf{k}} = d_x \sigma_x + d_y \sigma_y + d_0 I$  in terms of Pauli matrices has components:

$$\begin{aligned} d_x &= \frac{2t}{\sqrt{3}} \cos \left[ \frac{2\pi}{3N_s} (k_1 - k_2) \right] + \frac{4}{\sqrt{3}} \cos \left[ \frac{\pi}{N_s} (k_1 + k_2) \right] \cos \left[ -\frac{\pi}{3N_s} (k_1 - k_2) \right]; \\ d_y &= -\frac{2t}{\sqrt{3}} \sin \left[ \frac{2\pi}{3N_s} (k_1 - k_2) \right] + \frac{4}{\sqrt{3}} \cos \left[ \frac{\pi}{N_s} (k_1 + k_2) \right] \sin \left[ \frac{\pi}{3N_s} (k_1 - k_2) \right]; \\ d_0 &= \frac{2}{\sqrt{3}} \left\{ -\kappa \cos \left[ \frac{2\pi}{N_s} k_1 \right] - \mu \right\}. \end{aligned} \quad (4)$$

Using  $\gamma$  as our energy unit from now on, the free electrons part of the Matsubara action for Grassmanian fields  $\psi_{\mathbf{k}ln}^{*sI}$  is:

$$S^e = \frac{1}{T} \sum_{\mathbf{k}ln} \psi_{\mathbf{k}ln}^{*sI} \{ (-i\omega_n + d_{\mathbf{k}}^0) \delta^{IJ} + \sigma_i^{IJ} d_{\mathbf{k}}^i \} \psi_{\mathbf{k}ln}^{sJ}. \quad (5)$$

where  $\omega_n = \pi T (2n + 1)$  is the Matsubara frequency. The Green Function of free electrons has the matrix form

$$g_{\mathbf{k}n} = \{ (-i\omega_n + d_{\mathbf{k}}^0) I + \sigma_i d_{\mathbf{k}}^i \}^{-1} = \frac{(-i\omega_n + d_{\mathbf{k}}^0) I - \sigma_i d_{\mathbf{k}}^i}{(i\omega_n - d_{\mathbf{k}}^0)^2 - d_{\mathbf{k}}^{x2} - d_{\mathbf{k}}^{y2}}. \quad (6)$$

Now we turn to the spectrum of this model.

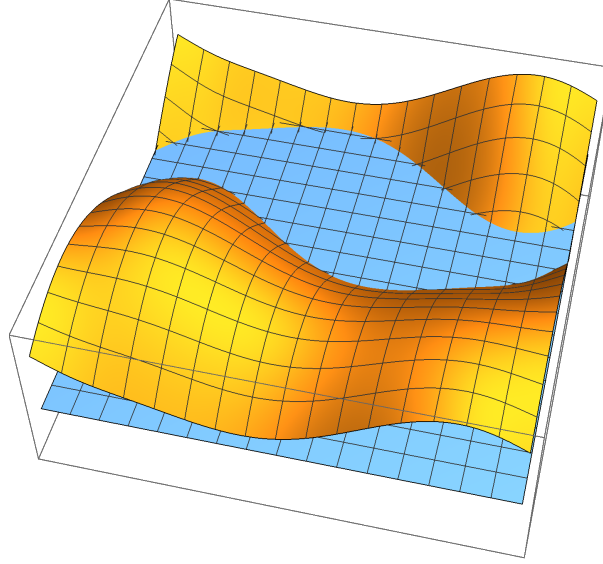


FIG. 2. The topological phase diagram of the Weyl semimetal at large tilt parameter ( $\kappa = 1.3$ ). Chemical potential (in units of  $\gamma = 500$  meV) is marked on each contour. The electron type I topology at low values of  $\mu$  undergoes transition to the type II at  $\mu = \mu_c^1 = 0.8$  meV. At yet larger  $\mu > \mu_c^2 = 1.35$ , the Fermi surface becomes again type I. This time the excitations are hole rather than electrons.

### The range of the topological type II phase at large $\kappa$

The spectrum of Hamiltonian of Eqs.(4) consists of two branches. The upper branch for  $\mu = 0.9eV$  is given in Fig. 2. The lower branch for a reasonable choice of parameters appropriate to  $MoTe_2$  is significantly below the Fermi surface and is not plotted. Blue regions represent the filled electron states. One observes a "river" from one boundary to the other of the Brillouin zone (in coordinates  $k_1$  and  $k_2$ , in terms of the original  $k_x, k_y$  it is a rhomb) characteristic to type II Fermi surface. Topologically this is akin to Fig.1b.

In Fig. 3 the Fermi surfaces in a wide range of densities  $n = 7. \times 10^{13} - 4.5 \times 10^{14} cm^{-2}$  are given. Topologically they separate into three phases. At chemical potentials below  $\mu_c^1 = 0.796 eV$ , corresponding to densities  $n < n_c^1 = 8. \times 10^{13} cm^{-2}$ , the Fermi surface consists of one compact electron pocket similar to Fig.1a, so that the electronic matter is of the ("customary") topological type I. The density is determined from the (nearly linear) relation between the

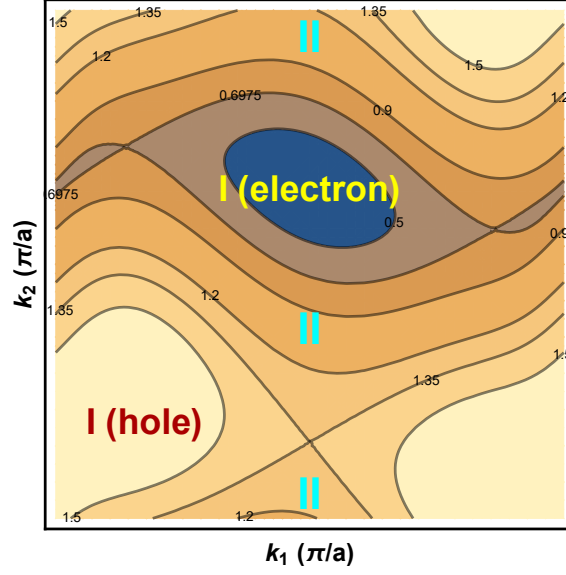


FIG. 3. Dispersion relation of WSM with  $\kappa = 1.3$ . The blue plane corresponds to chemical potential  $\mu = 0.8$  eV so that the Fermi surface has the type II topology.

chemical potential and density given in Fig. 4 (blue line, scale on the right). In the range  $\mu_c^1 < \mu < \mu_c^2 = 1.35$  eV the Fermi surface consists of two banks of a "river" (blue color represents filled electron states) in Fig.2 and can be viewed topologically as in Fig.1b and Fig.1c. The second critical density is  $n_c^2 = 3.6 \times 10^{14} \text{ cm}^{-2}$ . In this range the shape of both pieces of the Fermi surface largely does not depend on the density that is proportional to the area of the blue part of the surface.

To make this purely topological observation quantitative, we present in Fig. 4 (green line, scale on the left) the density of states (DOS) as a function of chemical potential. One observes that it is nearly constant away from the two topological I to II transitions where it peaks.

### Coulomb repulsion

The electron-electron repulsion in the layered WSM can be presented in the form,

$$V = \frac{e^2}{2} \sum_{\mathbf{n}l\mathbf{n}'l'} n_{\mathbf{n}l} v_{\mathbf{n}-\mathbf{n}',l-l'}^C n_{\mathbf{n}'l'} = \frac{e^2}{2N_s^2} \sum_{\mathbf{q}ll'} n_{\mathbf{q}l} n_{-\mathbf{q}l'} v_{\mathbf{q},l-l'}^C, \quad (7)$$

where  $v_{\mathbf{n}-\mathbf{n}',l-l'}^C$  is the "bare" Coulomb interaction between electrons with Fourier transform  $v_{\mathbf{q},l-l'}^C = v_{\mathbf{q}}^{2D} e^{-dq|l-l'|}$ ,  $v_{\mathbf{q}}^{2D} = 2\pi e^2 / q\epsilon$ . Here  $\epsilon$  is the dielectric constant of the intercalator material

The long range Coulomb interaction is effectively taken into account using the RPA approximation.

### SCREENING IN LAYERED WSM.

The screening in the layered system can be conveniently partitioned into the screening within each layer described by the polarization function  $\Pi_{\mathbf{q}n}$  and electrostatic coupling to carriers in other layers. We start with the former.

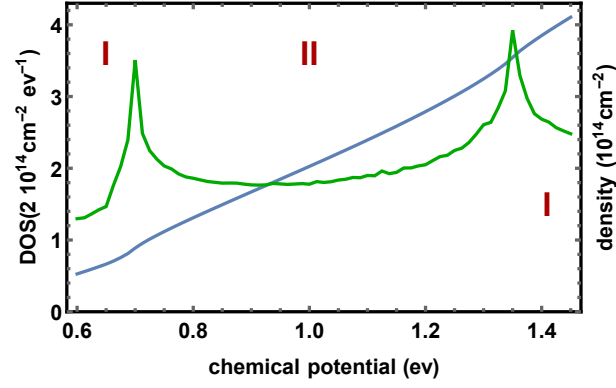


FIG. 4. Electron density and DOS as function of the chemical potential  $\mu$  of WSM with  $\kappa = 1.3$ . DOS has cusps at both I to II transitions. Between the transitions it is nearly constant in the range of densities from  $1.1 \times 10^{14}/\text{cm}^2$  to  $4. \times 10^{14}/\text{cm}^2$ .

#### Polarization function of the electron gas in Layered WSM

In a simple Fermi theory of the electron gas in normal state with Coulomb interaction between the electrons in RPA approximation the Matsubara polarization is calculated as a simple *minus* "fish" diagram [14] in the form:

$$\Pi_{\mathbf{q}n} = - \left( -2T \text{Tr} \sum_{\mathbf{p}m} g_{\mathbf{p}m} g_{\mathbf{p}+\mathbf{q},m+n} \right). \quad (8)$$

Using the GF of Eq.(6), one obtain:

$$\Pi_{\mathbf{q}n} = 4T \sum_{\mathbf{p}m} \frac{(i\omega_m + A)(i\omega_m + B) + C}{[(i\omega_m + A)^2 - \alpha^2][(i\omega_m + B)^2 - \beta^2]}, \quad (9)$$

where

$$\begin{aligned} A &= -d_{\mathbf{p}}^0; B = i\omega_n - d_{\mathbf{p}+\mathbf{q}}^0; \quad C = d_{\mathbf{p}}^x d_{\mathbf{p}+\mathbf{q}}^x + d_{\mathbf{p}}^y d_{\mathbf{p}+\mathbf{q}}^y; \\ \alpha^2 &= d_{\mathbf{p}}^{x2} + d_{\mathbf{p}}^{y2}; \quad \beta^2 = d_{\mathbf{p}+\mathbf{q}}^{x2} + d_{\mathbf{p}+\mathbf{q}}^{y2}. \end{aligned} \quad (10)$$

Performing summation over  $m$ , one obtains:

$$\Pi_{\mathbf{q}n} = - \sum_{\mathbf{p}} \left\{ \frac{\alpha^2 - \alpha(A-B) + C}{\alpha[(A-B-\alpha)^2 - \beta^2]} \tanh \frac{\alpha-A}{2T} + \frac{a^2 + \alpha(A-B) + C}{\alpha[(A-B+\alpha)^2 - \beta^2]} \tanh \frac{\alpha+A}{2T} \right. \\ \left. + \frac{\beta^2 + \beta(A-B) + C}{\beta[(A-B+\beta)^2 - \alpha^2]} \tanh \frac{\beta-B}{2T} + \frac{\beta^2 - \beta(A-B) + C}{\beta[(A-B-\beta)^2 - \alpha^2]} \tanh \frac{\beta+B}{2T} \right\}. \quad (11)$$

Now we turn to screening due to other layers.

#### Screening in a layered system

Coulomb repulsion between electrons in different layers  $l$  and  $l'$  within the RPA approximation is determined by the following integral equation:

$$V_{\mathbf{q},l-l',n}^{RPA} = v_{\mathbf{q},l-l'}^C + \Pi_{\mathbf{q}n} \sum_{l''} v_{\mathbf{q},l-l''}^C V_{\mathbf{q},l''-l',n}^{RPA}. \quad (12)$$

The polarization function  $\Pi_{\mathbf{q}n}$  in 2D was calculated in the previous subsection. This set of equations is decoupled by the Fourier transform in the  $z$  direction,

$$V_{\mathbf{q},q_z,n}^{RPA} = \frac{v_{\mathbf{q},q_z}^C}{1 - \Pi_{\mathbf{q}n} v_{\mathbf{q},q_z}^C}, \quad (13)$$

where

$$v_{\mathbf{q},q_z}^C = \sum_l v_{\mathbf{q}}^{2D} e^{iq_z l - qd|l|} = v_{\mathbf{q}}^{2D} \frac{\sinh[qd]}{\cosh[qd] - \cos[qd_z]}. \quad (14)$$

The screened interaction in a single layer therefore is given by the inverse Fourier transform [14]:

$$V_{\mathbf{q},l-l',n}^{RPA} = \frac{d}{2\pi} \int_{q_z=-\pi/d}^{\pi/d} e^{iq_z d(l-l')} \frac{v_{\mathbf{q},q_z}^C}{1 - \Pi_{\mathbf{q}n} v_{\mathbf{q},q_z}^C}. \quad (15)$$

Considering screened Coulomb potential at the same layer  $l = l'$ , the integration gives,

$$V_{\mathbf{q}n}^{RPA} = \frac{v_{\mathbf{q}}^{2D} \sinh[qd]}{\sqrt{b_{\mathbf{q}n}^2 - 1}}, \quad (16)$$

where  $b_{\mathbf{q}n} = \cosh[qd] - v_{\mathbf{q}}^{2D} \Pi_{\mathbf{q}n} \sinh[qd]$ . This formula is reliable only away from plasmon region  $b_{\mathbf{q}n} > 1$ . It turns out that to properly describe superconductivity, one can simplify the calculation at low temperature by considering the static limit  $\Pi_{\mathbf{q}n} \simeq \Pi_{\mathbf{q}0}$ . Consequently the potential becomes static:  $V_{\mathbf{q}}^{RPA} \equiv V_{\mathbf{q},n=0}^{RPA}$ .

## SUPERCONDUCTIVITY

Superconductivity in WSM is caused by a conventional phonon pairing. The leading mode is an optical phonon mode assumed to be dispersionless, with energy  $\Omega$ . The effective electron-electron attraction due to the electron-phonon attraction opposed by Coulomb repulsion (pseudo-potential) mechanism creates pairing below  $T_c$ . Further we assume the singlet  $s$ -channel electron-phonon interaction and neglect the inter-layers electrons pairing. In order to describe superconductivity, one should "integrate out" the phonon and the spin fluctuations degrees of freedom to calculate the effective electron-electron interaction. We start with the phonons. The Matsubara action for effective electron-electron interaction via in-plane phonons and direct Coulomb repulsion calculated in the previous Section. It is important to note that unlike in metal superconductors where a simplified pseudo-potential approach due to McMillan and other [15], in 2D and layered WSM, one has to resort to a more microscopic approach.

### Effective attraction due to phonon exchange opposed by the effective Coulomb repulsion

The free and the interaction parts of the effective electron action ("integrating phonons" + RPA Coulomb interaction) in the quasi-momentum - Matsubara frequency representation,  $S = S^e + S^{int}$ ,

$$S^{int} = \frac{1}{2T} \sum_{\mathbf{q}l'l'mm'} n_{\mathbf{q}ln} \left( \delta_{ll'} V_{\mathbf{q},m-m'}^{ph} + V_{\mathbf{q},l-l'}^{RPA} \right) n_{-\mathbf{q},-l',-n'}. \quad (17)$$

Here  $n_{\mathbf{q}ln} = \sum_{\mathbf{p}} \psi_{\mathbf{p}ln}^{*sI} \psi_{\mathbf{q}-\mathbf{p},l,n}^{sI}$  the Fourier transform of the electron density and  $S^e$  was defined in Eq.(5). The effective electron-electron coupling due to phonons is:

$$V_{\mathbf{q}m}^{ph} = - \left( \frac{\sqrt{3}}{2} \right)^2 \frac{g^2 \Omega}{\omega_m^2 + \Omega^2}, \quad (18)$$

where the bosonic frequencies are  $\omega_m^b = 2\pi mT$ .

### Gorkov Green's functions and the s-wave gap equations

Normal and anomalous (Matsubara) intra - layer Gorkov Green's functions are defined by expectation value of the fields,  $\langle \psi_{\mathbf{k}nl}^{Is} \psi_{\mathbf{k}nl}^{*s'J} \rangle = \delta^{ss'} G_{\mathbf{k}n}^{IJ}$  and  $\langle \psi_{\mathbf{k}nl}^{Is} \psi_{-\mathbf{k},-n,l}^{Js'} \rangle = \varepsilon^{ss'} F_{\mathbf{k}n}^{IJ}$ , while the gap function is

$$\Delta_{\mathbf{q}n}^{IJ} = \sum_{\mathbf{p}m} V_{\mathbf{q}-\mathbf{p},n-m} F_{\mathbf{p}m}^{IJ}, \quad (19)$$

where  $V_{\mathbf{q}n} = V_{\mathbf{q}n}^{ph} + V_{\mathbf{q}n}^{RPA}$  is a sublattice scalar. The gap equations in the sublattice matrix form are derived from Gorkov equations in Appendix B:

$$\Delta_{\mathbf{q}n} = - \sum_{\mathbf{p}m} V_{\mathbf{q}-\mathbf{p},n-m} g_{\mathbf{p}m} \{ I + \Delta_{\mathbf{p}m} g_{-\mathbf{p},-m}^t \Delta_{-\mathbf{p},-m}^* g_{\mathbf{p}m} \}^{-1} \Delta_{\mathbf{p}m} g_{-\mathbf{p},-m}^t. \quad (20)$$

In numerical simulation the gap equation was solved iteratively. Relatively large space cutoff  $N_s = 256$  is required. The frequency cutoff  $N_t = 128$  was required due to low temperatures approached. Typically 15 – 25 iterations were required. The parameters used were  $\Omega = 16meV$ . The electron - phonon coupling  $g = 20meV$ . Now we turn to results concentrating on two puzzling experimental results of ref.[6].

### Independence of $T_c$ on density in topological type II phase

In Fig.5 the critical temperature for various values of density are plotted. The blue points are for dielectric constant[6],  $\varepsilon = 16$ , describing the intercalated imidazole cations  $[C_2MIm]$  [17]. The inter - layer distance was kept at  $d = 10.5A$ .

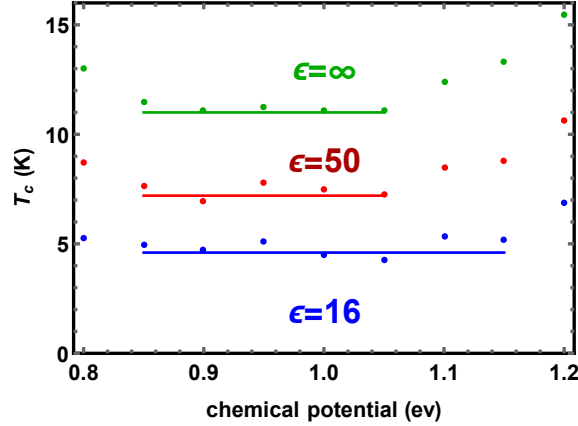


FIG. 5. Critical temperature of transition to superconducting state in type II layered WSM is shown as function of chemical potential (can be translated into carrier density via Fig.4). Three values of dielectric constant of the intercalant for fixed interlayer distance are shown. Parameters of the electron gas are the same as in previous figures.

The significance and generatization of the observation are discussed below.

### Increase of $T_c$ with dielectric constant of intercalator materials

The main idea of the paper is that the difference in  $T_c$  between different intercalators is attributed not to small variations in the inter - layer spacing  $d$ , but rather to large differences in the dielectric constant of the intercalating materials due to its effect on the screening. In experiment of ref.[6] the imidazole cations  $[C_2MIm]^+$  (1- ethyl - 3 - methyl - imidazolium) are short molecules[17] have  $\varepsilon = 16$ , while  $[C_6MIm]^+$  (1- hexyl - 3 - methyl - imidazolium) are long molecules[18] with a larger value  $\varepsilon \simeq 50$ . The inter - layer distance  $d$  is slightly dependent intercalators



changing from  $10.5\text{\AA}$  to  $11.7\text{\AA}$ . The blue points in Fig 5 describe a material with dielectric constant  $\epsilon = 16$  should. This is contrasted[18] with the  $\epsilon = 50$  material, see the red point. Neglecting the Coulomb repulsion, see the green points, critical temperature (a much simpler calculation of  $T_c$  in this case similar to that in ref.[11] is needed in this case) becomes yet higher. This demonstrate the importance of the Coulomb repulsion in a quasi 2D system. Superconductivity is weaker for monolayer on substrate since both air and substrate have smaller dielectric constants and hence weaker screen the Coulomb repulsion.

## DISCUSSION AND CONCLUSION

To summarize we have developed a theory of superconductivity in layered type II Weyl semi-metals that properly takes into account the Coulomb repulsion. The generalization goes beyond the simplistic pseudo - potential approach due to McMillan[15] and others and depends essentially on the intercalating material. The theory allows to explain the two puzzling phenomena observed recently in layered intercalated  $MoTe_2$  WSW compound [6]

The first experimental observation is that the gate voltage (changes in the chemical potential or equivalently in density) has no impact on critical temperature  $T_c$ . For the 3D density range  $8. \times 10^{20}cm^{-3} - 3.6 \times 10^{21}cm^{-3}$  the temperature changes within 5%. For the intercalating material  $[C_2MIm]^+$  with inter - layer distance  $d = 10.5\text{\AA}$  the 2D density range translates into  $8.4 \times 10^{13}cm^{-2} - 3.8 \times 10^{14}cm^{-2}$  with slightly larger spacings  $d = 11.7\text{\AA}$  shown in Figs 2-5. This feature is explained purely topologically, see schematic Fig.1. In the type II density range the shape of both pieces of the Fermi surface (the blue - yellow boundaries in Fig1b and Fig1c) largely does not depend on the density (that is proportional to the area of the blue part of the surface) leading, see Fig. 4 to approximate independence of the density of states (DOS)  $N(0)$  of chemical potential  $\mu$ . This feature is akin to the DOS independence on  $\mu$  for a parabolic (topologically type I like in Fig.1a) band in purely 2D materials, but has completely different origin.

Using the somewhat naive BCS formula

$$T_c \simeq \Omega e^{-N(0)g_{eff}^2}. \quad (21)$$

Here  $\Omega$  is the phonon frequency and  $g_{eff}$  the effective electron - phonon coupling. Assuming that both  $\Omega$  and  $g$  do not depend on the density one arrives at a conclusion that in the type II topological phase the critical temperature is density independent .

The second experimental observation[6] was that  $T_c$  is in fact very sensitive to the intercalating material. For imidazole cations  $[C_2MIm]^+$  the critical temperature is  $T_c = 4.2K$ , while for  $[C_6MIm]^+$  the temperature jumps to  $T_c = 6.6K$  or  $6.9K$  depending on the intercalation method. The inter - layer distance  $d$  is slightly dependent intercalators increasing from  $10.5\text{\AA}$  to  $11.7\text{\AA}$ . Our calculation demonstrates that the difference in  $T_c$  between different intercalators cannot be attributed to small variations in the inter - layer spacing  $d$ . On the contrary there are large differences in the dielectric constant of the intercalating materials. While  $[C_2MIm]^+$  have[17] a relatively small dielectric constant  $\epsilon = 16$ ,  $[C_6MIm]^+$  is estimated[18] in the range  $\epsilon = 40 - 60$ . Our theory accounts the difference in  $T_c$  due to changes in the screening of the Coulomb potential due to the inter - layer insulator.

## ACKNOWLEDGEMENTS.

This work was supported by NSC of R.O.C. Grants No. 101-2112-M-009-014-MY3.

## APPENDIX A. DETAILS OF THE MODEL

The system considered in the paper is fitted for the following values of the hopping and the tilt parameter. The dimensionless tilt parameter was taken from ref.[6]  $\kappa = 1.3$ . The hopping  $\gamma = 500 meV$  and  $t = 2$ . The calculations were performed on the discrete reciprocal lattice  $k_1, k_2 = 1, \dots, N_s$  with  $N_s = 256$ . Reciprocal lattice basis vectors are,

$$\mathbf{b}_1 = 2\pi \left(1, \frac{1}{\sqrt{3}}\right); \quad \mathbf{b}_2 = 2\pi \left(1, -\frac{1}{\sqrt{3}}\right), \quad (22)$$

so that a convenient representation is  $\mathbf{k} = \frac{k_1}{N_s} \mathbf{b}_1 + \frac{k_2}{N_s} \mathbf{b}_2$  with

$$k_x = \frac{2\pi}{N_s} (k_1 + k_2), \quad k_y = \frac{2\pi}{\sqrt{3}N_s} (k_1 - k_2). \quad (23)$$

## APPENDIX B. DERIVATION OF THE TWO SUBLATTICE GAP EQUATION

### Green's functions and the s-wave Gorkov equations

We derive the Gorkov's equations (GE) within the functional integral approach[19] starting from the effective electron action for grassmanian fields  $\psi^{*X}, \psi^Y$ .

$$S = \frac{1}{T} \left\{ \psi^{*X} (G_0^{-1})^{XY} \psi^Y + \frac{1}{2} \psi^{*Y} \psi^Y V^{YX} \psi^{*X} \psi^X \right\}, \quad (24)$$

where  $X, Y$  denote space coordinate, sublattices (pseudospin) and spin of the electron. Finite temperature properties of the condensate are described at temperature  $T$  by the normal and the anomalous Matsubara Greens functions for spin singlet state.

The GE in functional form are:

$$\langle \psi^A \psi^{*B} \rangle \frac{\delta}{\delta \psi^{*C}} \left\langle \frac{\delta S}{\delta \psi^{*B}} \right\rangle + \langle \psi^A \psi^B \rangle \frac{\delta}{\delta \psi^{*C}} \left\langle \frac{\delta S}{\delta \psi^B} \right\rangle = 0; \quad (25)$$

$$\langle \psi^A \psi^{*B} \rangle \frac{\delta}{\delta \psi^C} \left\langle \frac{\delta S}{\delta \psi^{*B}} \right\rangle + \langle \psi^A \psi^B \rangle \frac{\delta}{\delta \psi^C} \left\langle \frac{\delta S}{\delta \psi^B} \right\rangle = \delta^{AC}. \quad (26)$$

Performing the calculations and using the normal and anomalous Green functions in the form  $F^{AB} = \langle \psi^A \psi^B \rangle$ ;  $G^{AB} = \langle \psi^A \psi^{*B} \rangle$ , one obtains:

$$F^{AX} \left\{ (G_0^{-1})^{CX} - v^{XC} G^{CX} + v^{CX} G^{XX} \right\} + G^{AX} v^{XC} F^{XC} = 0. \quad (27)$$

Skipping second and third terms in bracket in this expression and defining, superconducting gap  $\Delta^{AB} = v^{AB} F^{AB}$ , one rewrites as a matrix products:

$$(G_0^{-1})^{CX} F^{XA} = G^{AX} \Delta^{XC}. \quad (28)$$

The first GE (multiplied from left by  $G_0$ ) is,

$$F^{AB} = -G^{AX} G_0^{BY} \Delta^{XY}, \quad (29)$$

while the second GE similarly is:

$$G^{AB} - G^{AX} \Delta^{XY} G_0^{ZY} \Delta^{*ZU} G_0^{UB} = G_0^{AB}. \quad (30)$$

### Frequency-quasi-momentum and the spin-sublattice decomposition

The generalized index  $A$  contains the space variables (space + Matsubara time,  $a$ ), spin  $s$  and the sublattice  $I$ . After performing the Fourier series with combined quasi - momentum - frequency  $\alpha$ :

$$\begin{aligned} F_{ab}^{s_1 s_2 IJ} &= \epsilon^{s_1 s_2} \sum_{\alpha} e^{i\alpha(a-b)} F_{\alpha}^{IJ}; \quad \Delta_{ab}^{s_1 s_2 IJ} = \epsilon^{s_1 s_2} \sum_{\alpha} e^{i\alpha(a-b)} \Delta_{\alpha}^{IJ}; \\ G_{0ab}^{s_1 s_2 IJ} &= \delta^{s_1 s_2} \sum_{\alpha} e^{i\alpha(a-b)} g_{\alpha}^{IJ}; \quad V_{ab}^{s_1 s_2 IJ} = \sum_{\alpha} e^{i\alpha(a-b)} v_{\alpha}. \end{aligned} \quad (31)$$

Substituting spins into Eq.(29,30), one obtains in the sublattice matrix form

$$\begin{aligned} F_\alpha &= -G_\alpha \Delta_\alpha g_{-\alpha}^t; \\ G_\alpha &= G_{0\alpha} \{I + \Delta_\alpha g_{-\alpha}^t \Delta_{-\alpha}^* G_{0\alpha}\}^{-1}, \end{aligned} \quad (32)$$

Convoluting the first GE by  $v_\nu$  one obtains:

$$\Delta_\omega = - \sum_\nu v_{\omega-\nu} G_\nu \Delta_\nu g_{-\nu}^t. \quad (33)$$

The solution of the second GE for  $G$  is:

$$G_\alpha = g_\alpha \{I + \Delta_\alpha g_{-\alpha}^t \Delta_{-\alpha}^* g_\alpha\}^{-1}. \quad (34)$$

Substituting into the first GE one obtain Eq.(20) in the text.

- 
- [1] Katsnelson M.I. 2012 *The Physics of Graphene*, (Cambridge, Cambridge University Press).
- [2] Soluyanov A. A. , Gresch D. ,Wang Z. ,Wu Q. ,Troyer M. ,Dai X. & Bernevig B. A. 2015, *Nature* **527**, 495.
- [3] Yu Z.-M. , Yao Y. , and Yang S. A. 2016 *Phys. Rev. Lett.* **117**, 077202.
- [4] O'Brien T. E. ,Diez M. , and Beenakker C. W. J. , 2016 *Phys.Rev. Lett.* **116**, 236401.
- [5] Wang C. et al. 2018 *Nature*, **555**, 231; Lin, Z. et al. 2018 *Nature*, **562**, 254; Huang H.,Zhou S. and DuanW., 2016 *Phys.Rev.B* **94** 121117; Yan M. et al, *Nature Comm.* 2017 **8**, 257; Furue Y. 2021 et al *Phys. Rev. B* **104**,144510.
- [6] Zhang H. , Rousuli A. ,Zhang K. ,Zhong H. ,Wu Y. ,Yu P. ,Zhou S. 2022 *2D Materials* **9** 045027.
- [7] Das Sarma S. andLi Q. 2013 *Phys. Rev. B* **88**, 081404(R);Brydon P.M.R. ,Das Sarma S. ,Hui H.-Y. and Sau J. D. 2014 *Phys. Rev. B* **90**, 184512;Li D. ,Rosenstein B. ,Shapiro B. Ya. , andShapiro I. 2014 *Phys. Rev. B* **90** 054517.
- [8] Fu L. and Berg E. 2010 *Phys. Rev. Lett.* **105**, 097001.
- [9] Zhang J.-L. et al. 2012 *Front. Phys.*, **7**, 193.
- [10] Alidoust M. , Halterman K. , and Zyuzin A. A. 2017 *Phys. Rev. B* **95**, 155124.
- [11] Li D. , Rosenstein B. , Shapiro B. Ya. , and Shapiro I. 2017 *Phys. Rev. B* **95**, 094513.
- [12] Shapiro B Ya , Shapiro I , Li D. and Rosenstein B. 2018 *J. Phys.:Condens. Matter* **30** 335403.
- [13] Wang S. T. et al. 2012 *Appl. Phys. Lett.* **101**, 183110.
- [14] Hawrylak P. , Eliasson G. , and Quinn J. J., 1988 *Phys. Rev. B* **37** 10187.
- [15] Bilbro G. and McMillan L. 1976 *Phys. Rev. B* **14** 1887.
- [16] Katayama S. ,Kobayashi A. ,Suzumura Y. 2006 *J. Phys. Soc. Japan* **75**, 054705;Goerbig M. O. , Fuchs J. -N.,Montambaux G. , Piéchon F. 2008 *Phys. Rev. B* **78**, 045415; Hirata M. et al. 2016 *Nature Commun.* **7** 12666.
- [17] Beal A R and Hughes H P 1979 *J. Phys. C: Solid State Phys.* **12** 881 .
- [18] Yang L., Fishbine B. H. , Migliori A. and Pratt L.R., 2010 *J. Chem. Phys.* **132** 044701.
- [19] Negele J.W. and Orlando H. , *Quantum Many Particle Systems*, 1998 Aspen, Advanced Book Classics, Westview Press.